Theses and Dissertations   1. Thesis and Dissertation Collection, all items

1994-06

A comparison of different control methods for vibration suppression of flexible structures using piezoelectric actuators

Feuerstein, Mark G.

Monterey, California. Naval Postgraduate School

http://hdl.handle.net/10945/30852

NAVAL POSTGRADUATE SCHOOL
Monterey, California

THESIS

A COMPARISON OF DIFFERENT CONTROL METHODS FOR
VIBRATION SUPPRESSION OF FLEXIBLE STRUCTURES
USING PIEZOELECTRIC ACTUATORS

by

Mark G. Feuerstein

June, 1994

Thesis Advisor: Brij N. Agrawal

Approved for public release; distribution is unlimited.

REPORT DOCUMENTATION PAGE			Form Approved OMB No. 0704-0188

1. AGENCY USE ONLY (Leave blank)	2. REPORT DATE June 1994	3. REPORT TYPE AND DATES COVERED Master's Thesis

4. TITLE AND SUBTITLE
A COMPARISON OF DIFFERENT CONTROL METHODS FOR VIBRATION SUPPRESSION OF FLEXIBLE STRUCTURES USING PIEZOELECTRIC ACTUATORS

5. FUNDING NUMBERS

6. AUTHOR(S)

Feuerstein, Mark G.

7. PERFORMING ORGANIZATION NAME(S) AND ADDRESS(ES)

Naval Postgraduate School

Monterey CA 93943-5000

8. PERFORMING ORGANIZATION REPORT NUMBER

9. SPONSORING/MONITORING AGENCY NAME(S) AND ADDRESS(ES)

10. SPONSORING/MONITORING AGENCY REPORT NUMBER

11. SUPPLEMENTARY NOTES

The views expressed in this thesis are those of the author and do not reflect the official policy or position of DOD or the US Government.

12a. DISTRIBUTION/AVAILABILITY STATEMENT

Approved for public release; distribution is unlimited.

12b. DISTRIBUTION CODE

A

13. ABSTRACT (Maximum 200 words)

This paper compares the use of Phase Lead control and Integral control methods to the Positive Position Feedback (PPF) method of suppressing the primary and secondary modes of vibration of a flexible structure. The basic characteristics of piezoelectric sensors and actuators are reviewed. Integral, Phase Lead, and PPF control methods are also reviewed. The Integral and Phase Lead control methods prove to be comparable to that of PPF while offering simpler implementation.

14. SUBJECT TERMS

Piezoelectric, Actuator, Control, PPF

15. NUMBER OF PAGES
56

16. PRICE CODE

17. SECURITY CLASSIFICATION OF REPORT	18. SECURITY CLASSIFICATION OF THIS PAGE	19. SECURITY CLASSIFICATION OF ABSTRACT	20. LIMITATION OF ABSTRACT
Unclassified	Unclassified	Unclassified	UL

i

A Comparison of Different Control Methods for
Vibration Suppression of Flexible Structures
Using Piezoelectric Actuators

by

Mark G. Feuerstein
Lieutenant Commander, United States Navy
B.S., Purdue University, 1981

Submitted in partial fulfillment
of the requirements for the degree of

MASTER OF SCIENCE IN ASTRONAUTICAL ENGINEERING

from the

NAVAL POSTGRADUATE SCHOOL
June 1994
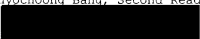
Author: _____
Mark G. Feuerstein

Approved by: _____
Brij N. Agrawal, Thesis Advisor

_____
Hyochoong Bang, Second Reader

_____
Daniel J. Collins, Chairman
Department of Aeronautical and Astronautical
Engineering

ii

ABSTRACT

This paper compares the use of Phase Lead control and Integral control methods to the Positive Position Feedback (PPF) method of suppressing the primary and secondary modes of vibration of a flexible structure. The basic characteristics of piezoelectric sensors and actuators are reviewed. Integral, Phase Lead, and PPF control methods of interest are also reviewed. The Integral and Phase Lead control methods prove to be comparable to that of PPF while offering a simpler implementation.

TABLE OF CONTENTS

I. INTRODUCTION

A. BACKGROUND

Structural designs of many disciplines are becoming larger while simultaneously attempting to meet ever more stringent weight and mass limits.   As this trend continues, the structural dynamics challenges associated with these designs become more difficult. Few if any disciplines exhibit these trends more dramatically than that of satellite design.

There exist any number of mission relatable tasks and environments that cause a satellite's structural modes of motion to be excited. Examples include, but are not limited to, antenna pointing, docking, and thermal response. Modern space structures, optimized for mass savings, can be described as "delicate" when considering modal responses to disturbances resulting from mission tasks and environments. The delicate nature of a modern spacecraft's modal response to excitation includes "flexibility" and "low damping".   Clearly, a versatile low mass method of controlling structural response to mission tasks and environments is desirable.

Controlling structural response requires both the capability to measure undesired motion and change it. Measurement of modal responses of flexible space structures

1

can best be accomplished by measuring strain vice acceleration due to the typically low frequencies involved.

Sensors available for this task include conventional strain gages, optical sensors, and piezoelectric ceramics. Piezoelectric ceramic sensors offer the most promise (Agrawal, 1992-3; Bailey, 1985; Crawley,1990; Hanagud, 1992; Tzou, 1989; and Venneri, 1993). Their features include (Betros, 1991):

- ease of implementation
- low temperature sensitivity
- high strain sensitivity
- low noise

Piezoelectric materials also lend themselves well to use as actuators in damping the modal responses of flexible space structures to mission task and environmental disturbances. Desirable features in meeting the requirements of an actuator include:

- low mass to preserve inherent structural configuration
- electrical operation
- wide bandwidth for controlling multiple modes
- internal force producer

Specifically, piezoelectric ceramic wafers (PZT) are an optimal choice for use as an actuator. As cited in (Betros, 1991) PZT's features include:

- near linear response
- adequate stiffness
- temperature insensitivity
- low electrical power consumption
- ease of implementation

Piezoelectric ceramic wafer technology has been utilized on the Naval Postgraduate School's Flexible Spacecraft Simulator (FSS) (Agrawal, 1992, Newman, 1992, Jones, 1991).

B. FOCUS OF THESIS

The effectiveness and utility of using piezoelectric sensors and actuators to control first mode vibrations of a cantilevered beam have been demonstrated (Newman, 1992). First and second mode vibration control has also been demonstrated (Bang and Agrawal, 1994). Both efforts made extensive use of Positive Position Feedback control methods. This effort compares the performance of the modified Positive Position Feedback (PPF) algorithm (Bang and Agrawal, 1994), to Phase Lead and Integral approaches using digital compensators. Both single and multiple mode damping performance will be examined.

II. THEORY

A. PIEZOELECTRIC

1. Classical Practice

Piezoelectricity (translated as "pressure electricity") is the ability of certain crystalline materials to develop an electrical charge proportional to mechanical strain or deformation (i.e., an electric polarization and corresponding voltage is induced due to the displacement of charged atoms along the axis of deformation). The charge is directly proportional to the amount of strain, and changes sign between compression and tension. The piezoelectric effect is linear with respect to the applied field within the elastic limit. Conversely, when an electric field is applied to such a crystal, the crystal becomes deformed or strained by an amount proportional to the applied field.

Piezoelectric interaction requires that certain axes of the medium exhibit "one-way" characteristics or polarity. Such polarity is inherent in some crystal classes, yet naturally absent in other crystal classes and in isotropic (lacking predetermined axes; similar characteristics in all directions) materials.

Until the mid 1940s, the study of piezoelectricity had been a branch of crystal physics. Since then, it has been

4

known that naturally isotropic ceramic materials can be caused
to exhibit piezoelectric characteristics by exposing them to
strong electric fields (on the order of 50 Volts/mil). The
process of generating piezoelectric properties in isotropic
ceramic materials is called "poling", and is analogous to
magnetizing a permanent magnet. Interestingly, such diverse
media as wood and wax demonstrate weak piezoelectric effects.

In classical practice, piezoelectric devices tend to
be limited to applications involving small displacements and
small amounts of electric charge per cycle. Jaffe (Jaffe,
1971) states

> the limited charge density and strain amplitude of
> piezoelectrics makes them unattractive for low
> frequency applications.

Piezoelectric devices tend to become increasingly useful with
increasing frequency due to the fact that electric current is
proportional to charge times frequency.

Given this classical bias away from low frequency,
large amplitude applications, many early applications
exhibited predictably higher frequency characteristics.
Examples include phonograph pickups and instrument transducers
such as those used in blood vessels to record periodic changes
in blood pressure associated with the cycle of heart beats.

It is only relatively recently that attempts have been
made to apply piezoelectric components to lower frequency,
larger amplitude applications.

2. Piezoelectric Properties

Piezoelectric ceramics tend to have relatively high dielectric constants (ratio of material's permittivity to that of free space). The piezoelectric effect demonstrated by these materials can be classified as *direct* or *converse*. Recall that in ordinary solid materials, the stain caused by a stress is related by a modulus of elasticity. Piezoelectricity is the creation of charge by strain resulting from applied stress. In the direct effect, the charge is proportional to the force, and of different sign for tension and compression. A piezoelectric constant D may be defined as proportional to the charge per unit area, Q/A, and the stress, T where:

$$Q/A = DT \qquad (1)$$

Here, the constant D has units of Coulombs per newton. In the converse effect, an applied electric field ϕ results in a proportional strain, ϵ, where expansion or contraction depends on polarity. In this case, D has units of meters/volt, and is related to strain and applied field by:

$$D = \epsilon/\phi \qquad (2)$$

Of course, the units of Coulombs per Newton and meters per volt are equivalent. The numerical value of D is equal in both cases. Large values of D are desired in materials used to develop motion or vibration.

It should be noted that for many ceramics and crystals, the elastic, dielectric, and piezoelectric constants are dependent on the axes of the material.

Finally, an indicator of the strength of material's piezoelectric effect is the value of the electromechanical coupling factor, k (not to be confused with the dielectric constant K). It measures the fraction of electrical energy converted to mechanical energy (or vice versa) when a crystal or ceramic is stressed.

The properties of piezoelectric ceramics as defined by the dielectric, piezoelectric, and elastic coefficients are all functions of the state of polarization. They are amplitude dependent and become non-linear and even non-reversible when the applied stress or field exceeds the limits of the material (extreme stress or field strength can "depole" the ceramic). The dielectric and elastic coefficients have both real and imaginary or dissipative components.

B. SENSORS

As outlined in Chapter I.B, piezoelectric ceramic sensors enjoy many desirable features including high sensitivity. Piezoelectric ceramic sensors are approximately 10^5 times more sensitive than conventional strain gages.

Figure 1 below illustrates the sensor mode of a piezoelectric ceramic wafer. The illustration on the left side of the figure shows vertical expansion and lateral

7

contraction when a the wafer is subjected to vertical tension.
The applied force produces voltage of opposite polarity to
that of the poling voltage. The right illustration
demonstrates the case where the wafer is subject to vertical
compression. The applied force produces voltage of the same
polarity as that of the poling voltage.

Figure 1. PZT sensor mode.

Piezoelectric sensors produce a charge Q_s when strained laterally as given by:

$$Q_s = AEd_{31}(\epsilon_1 + \epsilon_2) \qquad (3)$$

where d_{31} is the lateral strain coefficient of the material, A is the lateral area, E is Young's modulus, and ϵ_1 and ϵ_2 represent strain in the longitudinal and transverse directions respectively.

Sensor capacitance C_s is given by:

$$C_s = DA/t_s \qquad (4)$$

where D is the dielectric constant or permittivity and t_s is the thickness of the sensor. Thus, the output voltage V_o is given by:

$$V_o = t_s(Ed_{31}/D)(\epsilon_1 + \epsilon_2) \qquad (5)$$

Of course, the longitudinal strain ϵ_1 and the lateral strain ϵ_2 can be related by poison's ratio v as given by:

$$\epsilon_1 v = -\epsilon_2 \qquad (6)$$

Thus, equation (5) can be written as:

$$V_o = t_s(Ed_{31}/D)(1-v)\epsilon_1 \qquad (7)$$

Values for the material constants cited above are given in Table I for the Navy Type II piezoelectric ceramic sensor used on the FSS.

Table I. MATERIAL CONSTANTS FOR NAVY TYPE II PZT.

Quantity	Description	Units	Value
d_{31}	Lateral Strain	m/V or Coul/N	1.8e-10
E	Young's Modulus	N/m^2 or Pascal	6.30e10
v	Poison's Ratio	N/A	0.35
D	Abs Permittivity	Farad/m or N/V^2	1.5e-8
t_s	Sensor Thickness	m	1.905e-4
t_b	Beam Thickness	m	1.5877e-3
A	Sensor Area	m^2	6.452e-4

Thus, the PZT sensor will produce 0.1436 Volts/μ-strain when accounting for ϵ_1 and ϵ_2, and 0.0933 when using Poisson's ratio and measuring only ϵ_1.

C. ACTUATORS

Piezoelectric ceramic actuators, as highlighted in Chapter I.A, feature high stiffness, linearity, and easy implementation. Figure 2 below illustrates the actuator mode of a piezoelectric ceramic wafer. The illustration on the left side of the figure demonstrates vertical expansion and lateral contraction when a voltage of the same polarity as the poling voltage is applied to the ceramic. The right side illustration demonstrates the case where the applied voltage is of opposite polarity from the poling voltage.
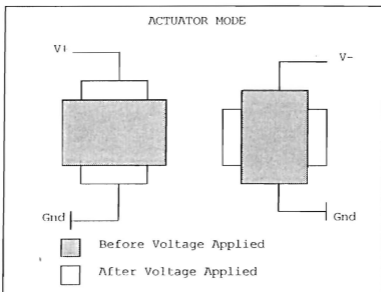
10

Figure 2. PZT actuator mode.

Applying a voltage **V** to a piezoelectric ceramic wafer produces an electric field Φ across the wafer denoted by:

$$\Phi = V/t_a \tag{8}$$

Lateral strain is developed from the applied voltage according to the relation:

$$\epsilon = d_{31}\Phi \tag{9}$$

Equation **(9)** can be rewritten as:

$$\epsilon = d_{31}V/t_a \tag{10}$$

The stress resulting from the voltage induced strain is

11

determined by Young's modulus $\overset{\mathcal{E}}{\underset{\vee}{}}$ and the resulting linear force

F can be determined from the stressed area. Hence, the force

developed by the application of voltage to the PZT is:

$$F = bEd_{31}V \qquad (11)$$

where **b** is the width of the actuator wafer. It follows that

the moment **M** developed is given by:

$$M = bEd_{31}(t_a/2 + t_b/2)V \qquad (12)$$

where t_b represents the thickness of the beam to which the PZT

actuator is attached. Using the numerical values of the

material constants found in Table I, the applied voltage **V**

develops moment **M** Newton-meters according to:

$$M = (2.5609e-4)V \qquad (13)$$

The force **F** in Newtons is given by:

$$F = (0.288)V \qquad (14)$$

The numerical values were derived using the dimensions of the

Navy Type II PZT wafers used in the experiment.

D. POSITIVE POSITION FEEDBACK

Positive Position Feedback (PPF) control methods (Betros,

1991) are applied by feeding the structural position

coordinate directly to the compensator, and the product of the

compensator and a scalar gain factor positively back to the

structure. The equations of motion describing PPF are:

$$\text{Structure} \quad \ddot{\xi} + 2\zeta\omega\dot{\xi} + \omega^2\xi = g\omega^2\eta \qquad (15)$$

$$\text{Compensator} \quad \ddot{\eta} + 2\zeta_c\omega_c\dot{\eta} + \omega_c^2\eta = \omega_c^2\xi \qquad (16)$$

12

where

      ξ is the modal coordinate of the structure

      ω is the structural resonant frequency

      ζ is the structural damping ratio

      η is the modal coordinate of the compensator

      ω_c is the compensator resonant frequency

      ζ_c is the compensator damping ratio

      g is the positive scalar gain factor of the feedback term

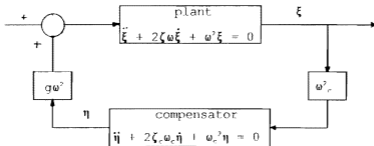A representative PPF control diagram is shown in Figure 3 below.

Figure 3. Control diagram for PPF feedback.

13

The following points should be considered when using Positive Position Feedback control methods:

- Large gain in the damping region
- Easy to implement
- Will add flexibility at low frequency (could induce static instability if gain too high)

Figure 4 below illustrates the basic block diagram for the PPF, Integral, and Phase Lead controllers.
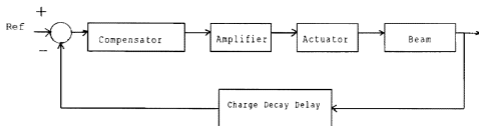

Figure 4. Basic controller block diagram.

A reference signal (value=0) is chosen commensurate with the vibration control objective. The compensator block represents either the PPF, Phase Lead, or the Integral controllers as shown in Figures 5, 6, and 7 respectively, below.
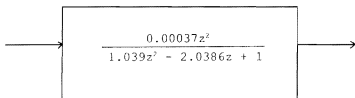
14

$$\frac{0.00037z^2}{1.039z^2 - 2.0386z + 1}$$

Figure 5. PPF compensator block detail in z domain, T=0.02 seconds sampling period.

$$\frac{1.0076z - 1}{1.134z - 1}$$
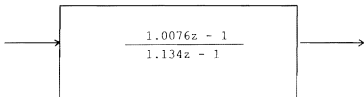
Figure 6. Phase Lead compensator block detail in z domain, T=0.02 seconds sampling period.
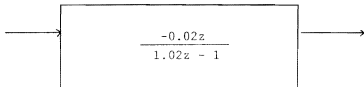

$$\frac{-0.02z}{1.02z - 1}$$

Figure 7. Integral compensator block detail in z domain, T=0.02 seconds sampling period.

The compensator's signal is sent to a power amplifier before being received by the piezoelectric actuator. The beam is then acted upon by the actuator; the actuator produces a bending moment at both ends of the actuator. A signal, generated by a piezoelectric sensor is fed back via a charge decay delay block to the compensator. The charge delay decay block, shown in Figure 8, is required because charge from the piezoelectric sensor tends to decay before the information it represents is conveyed, due to the low first mode natural frequency of vibration (approximately 0.15 Hz) of the beam. This decay produces sensor output that is close to the strain rate of the structure. Since the desired control variable is position, the sensor output must be converted into position information. Thus, the charge decay delay block output is position information.
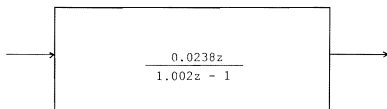
$$\frac{0.0238z}{1.002z - 1}$$

Figure 8. Charge decay delay block detail in z domain, T=0.02 seconds sampling period.

The complete PPF system block diagram, as represented by the AC-100, a real time controller, used to control the FSS, is shown below in Figure 9.

Figure 9. PPF AC-100 block diagram.

18

E. PHASE LEAD CONTROL

1. Phase Lead Control Theory

Phase lead compensation is similar to derivative control except that a first order pole is added to the denominator of the transfer function as shown below.

$$G(s) = (s + \alpha) / (s + \beta) \tag{17}$$

In this case, α is less than β. The advantage of this approach is that amplification of the compensation magnitude at high frequencies is limited to a certain level (Franklin, 1991).

While a pure derivative control compensator theoretically can provide 90 degree phase angle compensation for all modes, a phase lead controller can only approach 90 degrees for a band of frequencies depending upon the characteristics of the transfer function. Usually, the phase angle is maximized at a specific frequency, and decreases for other frequencies. The parameter $1/\alpha$ is referred to as the lead ratio. However, increasing or decreasing values of α can lead to undesirable increases in the amplification of the compensation magnitude. Thus, it is important to select values for α that yield acceptable phase margins for different flexible modes without amplifying noise at high frequencies.

The complete Phase Lead control block diagram, as represented by the AC-100, a real time controller, used to control the FSS, is shown below in Figure 10.
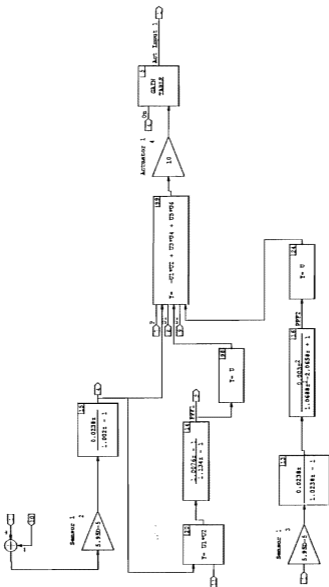
19

Figure 10. Phase Lead control AC-100 block diagram.

20

2. **Phase and Gain representations of Phase Lead and PPF
    Control**

Representative magnitude and phase angle plots for
Phase Lead and PPF compensators are shown below in Figures 11
and 12.

The Phase Lead phase angle relationship for the
specific Phase Lead case studied is represented by:

$$\Phi(\omega) = \tan^{-1}(\omega/\alpha) - \tan^{-1}(\omega/\beta) \qquad (18)$$

where α and β are user defined controller parameters, and the
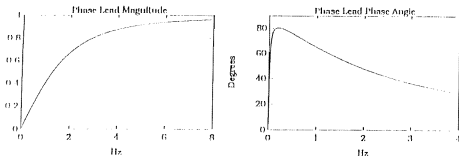input value ω represents the structural frequency of the beam.

Figure 11. Phase Lead magnitude and phase angle.

Figure 11 above represents Phase Lead control magnitude. It is seen that the magnitude approaches a value of one as the frequency increases. Again, a pure derivative controller would experience continuously increasing values as frequency increases which tends to amplify noise present in signals.

Figure 11 above also shows Phase Lead control phase angle response. It is seen that phase angle can be intentionally maximized in the region surrounding the beam's natural frequency of 0.15 Hz. The transfer function can be modified to change the shape of this curve to include a broader range of frequencies for desired phase angle magnitudes under the plateau. Obviously, controller performance at frequencies outside of this optimum range would be degraded.
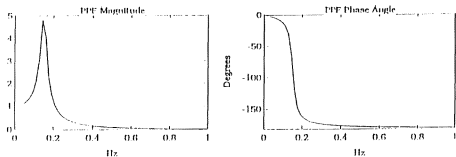

Figure 12. PPF magnitude and phase angle.

Figure 12 above represents a PPF controller's magnitude response. Note the sharp peak in magnitude at the intended frequency. This is the essential characteristic of a PPF controller's capability to be tuned to a single frequency, hence its good performance in quickly controlling single modes.

Figure 12 above also shows a PPF controller's phase angle response. The phase angle crosses 90 degrees at the beam's natural frequency. Each mode of the beam would require an individually tailored PPF compensator, thus each mode would be damped at a 90 degree induced phase angle.

F. INTEGRAL CONTROL

1. Integral Control Theory

Integral control is another popular classical control method. The primary reason for using integral control is to mitigate steady state errors, or to increase low frequency attenuation capability. This approach enjoys the added advantage of increased system performance at the expense of stability margin. This takes the form of increased tolerance of control gains. A representative transfer function is:

$$G(s) = k/Ts \qquad (19)$$

where T is called integral or reset time and $1/T$ is the reset rate.

Integral controllers can experience degraded performance if used with actuators of limited dynamic range

23

(as all real actuators are). The integrator tends to build large values in response to nonsymmetric or constant inputs which saturate the physical actuators. The net effect can be reduced controller effectiveness. Integral controllers can also build a bias if left activated for long periods of time. This is due to the integration of small but unavoidable system noise signals. An effective method of mitigating this effect is to activate the integral controller only when required with minimal deviation from pure integral action.

The complete Integral control block diagram used to control the FSS, as represented by the AC-100, is shown below in Figure 13.

Figure 13. Integral control AC-100 block diagram.

2. Integral Control Phase and Gain Representations

The actual function used in for the Integral controller was:

$$G(s) = k/T(s + \alpha) \qquad (20)$$

where α is introduced to prevent actuator saturation caused by pure integral action upon the input signal.

The Integral controller phase angle is given by the following:

$$\Phi(\omega) = \tan^{-1}(\omega/\alpha) \qquad (21)$$

where α is a user defined controller parameter, and the input value ω represents the structural frequency of the beam.

Representative magnitude and phase angle examples are given below in Figure 14.
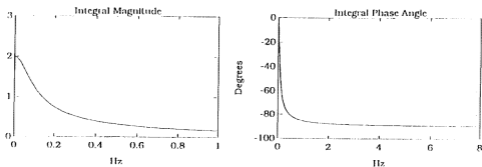

Figure 14. Integral control magnitude and phase angle.

Figure 14 above represents Integral control magnitude response. It is seen that the magnitude begins at $|G_c(j\alpha)|$ and approaches zero with increasing frequency.

Figure 14 above also shows Integral control phase angle response. The response begins at 0 degrees and decreases to approach -90 degrees. Observe that phase angle contribution is chosen such that it is maximized in the region around the first mode natural frequency of the structure.

III. EXPERIMENTAL ANALYSIS

A. PHYSICAL CONFIGURATION

The experiment makes use of the Naval Postgraduate School's Flexible Spacecraft Simulator (FSS). The physical setup of the experiment is shown below in Figure 15. The main body of the FSS, the large disk, is fixed with respect to the granite table. The 'L' shaped flexible arm is the only element of the experiment that is subject to vibrational motion. It is supported by air pads located at the elbow joint and one end of the 'L' shaped arm. The other end of the arm is fixed to, and supported by, the fixed main body. The air pads allow the arm to move in an essentially frictionless environment given that the granite table is kept essentially dust free.

The piezoelectric sensors and actuators used in this experiment are located at the end of the arm that attaches to the main body as shown in Figure 16. Pairs of sensors and actuators are mounted immediately adjacent to one another on either side of the beam. Previous studies have shown that the potential phase error due to nearly collocated sensors/actuators is negligible. The ceramic elements are mounted such that their individual polarities are

complementary. The placement of the sensors and actuators has
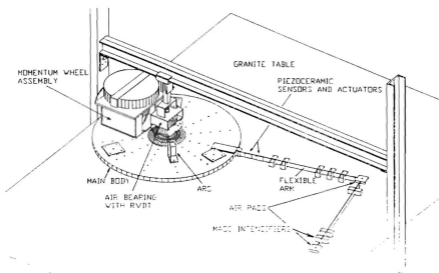been previously developed (Jones, 1991).

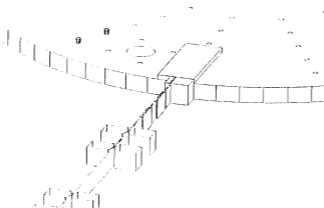Figure 15. Flexible Spacecraft Simulator (FSS).

Figure 16. Piezoelectric sensor and actuator placement.

The beams' dynamic characteristics were modified into the desired dynamic system model by the placement of concentrated masses on both sides of the beams along their length. The resulting first mode natural frequency is approximately 0.15 Hz.

B. EXPERIMENTAL PROCEDURE

The procedure was to explore the performance of different control approaches using a digital controller and comparing the results to those obtained previously (Bang and Agrawal, 1994), from the "modified" PPF approach. The same flexible arm configuration was used.

Open and closed loop runs were performed. Most of the runs attempted to excite the arm's first mode of vibration without measurably exciting higher modes. However, many runs did have multiple mode excitation as an objective.

The Phase Lead phase angle relationship was also examined using:

$$\phi(\omega) = \tan^{-1}(\omega/\alpha) - \tan^{-1}(\omega/\beta) \qquad (22)$$

where α and β are user defined controller parameters, and the input value ω represents the structural frequency of the beam.

The phase angles between sensors and actuators ranged between 60 degrees and 88.9 degrees. The results are discussed in section III.C below.

Data was obtained by monitoring the sensors' and actuators' output using a Hewlett-Packard oscilloscope, and the Real Time Monitor feature of the AutoCode MatrixX software package as installed on an AC-100/VAX workstation.

The primary performance indicator used for comparison between PPF and Phase Lead methods was damping ratio, ζ.

31

The damping ratio, ζ, was calculated by the log decrement method:

$$\zeta = (1/2\pi n)\ln(A_i/A_f) \qquad (23)$$

where A_i is the initial amplitude, A_f is the final amplitude, and n is the number of cycles between the two amplitudes measured. The observed damping ratios were small enough to assume that the damped frequency and the natural frequency were essentially equal.

C. EXPERIMENTAL RESULTS

1. Positive Position Feedback (PPF) Controller

A modified version of the PPF controller was developed and discussed previously (Bang and Agrawal, 1994). Those results are repeated here for later comparison to the Phase Lead Controller discussed below. Open and closed loop responses of the modified PPF controller for first and higher order modes are presented in Figures 17 and 18 respectively. The observed open loop first mode damping ratio was 0.0142. The observed closed loop first mode damping ratio was 0.0408, a 187% increase in damping. The observed open loop multimode damping ratio was 0.0183. The observed closed loop multimode damping ratio was 0.0489, a 167% increase in damping.
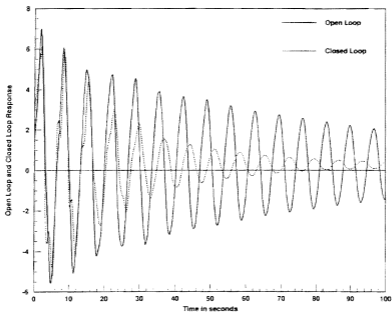
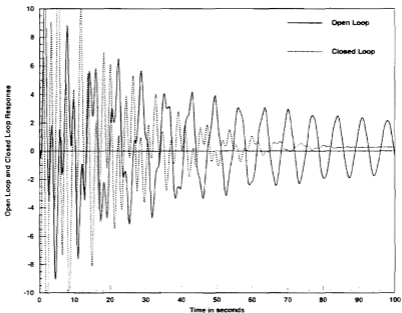Figure 17. PPF controller first mode performance.

33

Figure 18. PPF controller multimode performance.

It should be noted that the best PPF multimode response was obtained by damping only the first mode. Attempts to control the second mode tended to degrade overall damping performance.

34

2. Phase Lead Controller

Phase lead controllers with sensor-actuator phase angles approaching 90 degrees were first attempted. However, choosing controller gains low enough so as not to cause instability in the arm's response, resulted in unacceptably low damping ratios as shown in Figures 19 and 20. Again, the observed first mode open loop damping ratio was 0.0142. The observed first mode closed loop damping ratio was 0.0202, a 42% increase in damping. The phase angle was 88.88 degrees. Again, the observed multimode open loop damping ratio was 0.0183. The observed multimode closed loop damping ratio was 0.0241, a 32% increase in damping. The phase angle was 88.88 degrees.
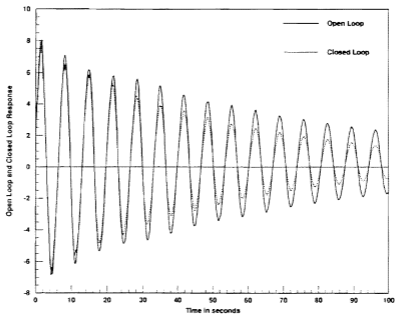
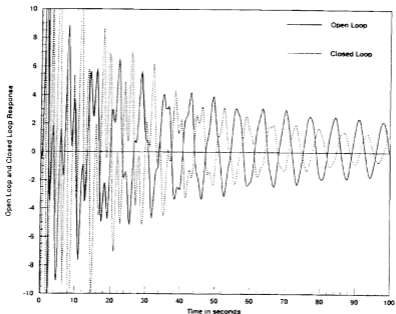Figure 19. Phase Lead controller first mode performance.

Figure 20. Phase Lead controller multimode performance.

The sensor-actuator phase angle relationship was then
reduced to 60 degrees.   This allowed the use of higher
controller gains, while preserving the controller's ability to
damp higher order modes.   Figure 21 shows favorable
performance. Again, the observed first mode open loop damping
ratio was 0.0142. The observed first mode closed loop damping

ratio was 0.0243, a 71% increase in damping. The phase angle
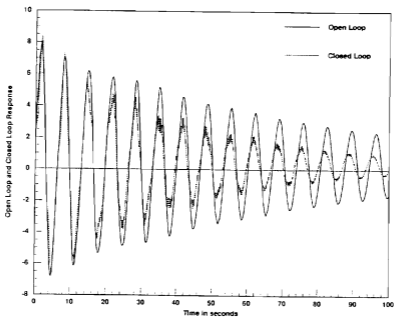was 60 degrees.

Figure 21. Phase Lead controller first mode performance.

The phase lead controller's performance in damping higher
order modes of motion was also examined. The open and closed

loop results are shown in Figure 22. The observed multimode
open loop damping ratio was 0.0183. The observed closed loop
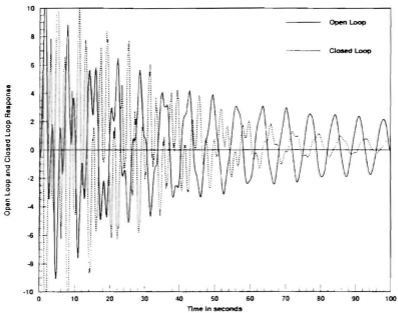damping ratio in was 0.0367, a 100% increase in damping.

Figure 22. Phase Lead controller multimode performance.

3. Integral (Phase Lag) Controller

An Integral (phase lag) controller was originally investigated with unsatisfactory results. It was determined that continuous activation of the controller was allowing integration of small system biases, resulting in degraded controller performance. A modified approach was undertaken whereby the actuator was not activated until immediately before it was required. The results then proved to be favorable for both first and multimode cases. Figure 23 illustrates the first mode results. The observed first mode open loop damping ratio was 0.0142. The observed closed loop damping ratio was 0.034, a 139% increase in damping. Figure 24 illustrates the multimode results. The observed multimode open loop damping ratio was 0.0183. The observed closed loop damping ratio was 0.0367, a 100% increase in damping.
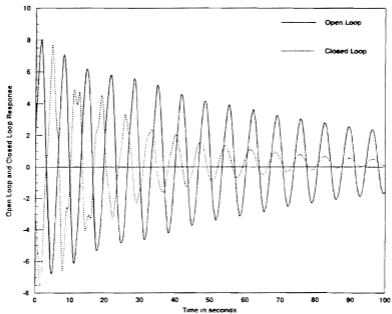
Figure 23. Integral controller first mode performance.
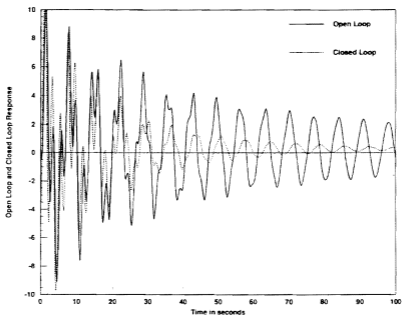
Figure 24.   Integral controller multimode performance.

The results, measured as damping ratios, ζ, are summarized
in Table II below.

Table II. OBSERVED DAMPING RATIOS.

Control Mode	Open Loop ($1^{st}/2^{nd}$ Mode)	Closed Loop (First Mode)	Closed Loop Higher Modes
Modified PPF	0.0142/0.0183	0.0408	0.0489
Phase Lead ($\Phi=90^{0}$)	0.0142/0.0183	0.0202	0.0241
Phase Lead ($\Phi=60^{0}$)	0.0142/0.0183	0.0243	0.0367
Integral	0.0142/0.0183	0.034	0.0367

IV.   CONCLUSIONS

As was shown by Newman, (Newman, 1992), PPF works very well for quickly damping a single mode when the structural characteristics of the beam are well known and closely modelled. However, developing a model can be expensive and time consuming.   Where this is the case, Phase Lead or Integral controller strategies can be useful.   Favorable performance can be obtained without resorting to involved structural modelling.

Both the Integral and Phase Lead methods also appear to be useful in damping higher order modal vibration. However, the Phase Lead can suffer reduced system stability as phase lead angles are reduced. Series connection of single Phase Lead compensators is recommended to enhance phase angle contribution to higher flexible modes.   The PPF can damp higher order modes, but a single compensator is required for each controlled mode.

Phase Lead techniques can realize their full potential given further study in the areas of increased stability margins, and using higher gains which improve performance, with stability guarantees. Each of the techniques may benefit from continuous real time scheduling of controller gains to maximize actuator action within the actuator saturation limit. Further study may also be warranted in developing a simple

44

grid based mechanical release method to facilitate consistent flexible arm release positions and forces, thus further improving data quality.

V. POTENTIAL APPLICATIONS

The potential applications of this promising technology are limitless. In the past, piezoelectric ceramics have been used primarily in high frequency applications. From medical technology, to sonar transducers, to 1940's vintage phonograph needles, PZT ceramics have seen wide use. The Naval Postgraduate School's Flexible Spacecraft Simulator continues to explore the challenging low frequency and high strain level application of these versatile devices.

With the advent of smaller computers and power supplies, so called micro-controllers, active control systems will find their way into more challenging "system" oriented structural and non structural applications.

LIST OF REFERENCES

Agrawal, B.N., Bang, H., and Hailey, J., *Application of Piezoelectric Actuators and Sensors in the Vibration Control of Flexible Spacecraft Structures*, IAF 92-0319, World Space Congress, Washington D.C., 28 Aug. - 5 Sept. 1992.

Agrawal, B.N., and Bang., H., *Active Vibration Control of Flexible Space Structures by using Piezoelectric Sensors and Actuators*, Proceedings for the 14th Biennial ASME Conference, Albuquerque, NM, Sept. 19-22, 1993, pp.169-179.

Bailey, T., and Hubbard, J.E., "Distributed Piezoelectric Polymer Active Vibration Control of a Cantilever Beam", *Journal of Guidance, Control, and Dynamics*, Vol. 8, No. 5, 1985, pp. 605-611.

Bang, H., and Agrawal, B.N., *A Generalized Second Order Compensator Design for Vibration Control of Flexible Structures*, Proceedings on 35th Structures, Structural Dynamics and Materials Conference, Hilton Head, SC, April 21-22, 1994.

Betros, R.S., and Bronowicki, A.J., "Seminar Notes," *Active Damping Workshop*, Spring, 1991.

Crawley, E.F., and Anderson, E.H., *Detailed Models of Piezoelectric Actuation of Beams*, Journal of Intellectual Material Systems and Structures, Vol. 1, Jan. 1990, pp. 4-25.

Franklin, G.F., and Powell, J.D., and Emami-Naeini, A., *Feedback Control of Dynamic Systems*, Addison Wesley, 1991.

Hanagud, S., Obal, M.W., and Calise, A.J., "Optimal Vibration Control by the Use of Piezoceramic Sensors and Actuators", *Journal of Guidance, Control, and Dynamics*, Vol. 15, No. 5, Sept-Oct, 1992, pp. 199-1206.

Jaffe, B., *Piezoelectric Ceramics*, McGraw Hill Book Co., 1971.

Jones, E.S., *Development of an Active Damping System to Aid in the Attitude Control of Flexible Spacecraft*, Master's Thesis, Naval Postgraduate School, Monterey, CA, 1991.

Newman, S., *Active Damping Control Of A Flexible Space Structure Using Piezoelectric Sensors And Actuators*, Master's Thesis, Naval Postgraduate School, Monterey, California, 1992.

Tzou, H.S., and Gadre, M., *Theoretical Analysis of a Multi-Layered Thin Shell Coupled with Piezoelectric Shell Actuators for Distributed Vibration Controls,* Journal of Sound and Vibration, Vol. 132, No. 3, 1989, pp. 433-450.
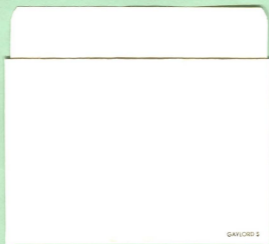
Venneri, S.L. and Wada, B.K., *Overview of NASA's Adaptive Structures Program,* IAF 93-I.5.243, 44th Congress of the International Astronautical Federation, Graz, Austria, Oct 16-22, 1993.

INITIAL DISTRIBUTION LIST

1. Defense Technical Information Center   2
   Cameron Station
   Alexandria, VA 22304-6145

2. Library, Code 52   2
   Naval Postgraduate School
   Monterey, CA 93943-5002

3. Chairman, Code AA   1
   Department of Aeronautics and Astronautics
   Naval Postgraduate School
   Monterey, CA 93943

4. Chairman, Code SP   1
   Department of Aeronautics and Astronautics
   Naval Postgraduate School
   Monterey, CA 93943

5. Professor Brij N. Agrawal, Code AA/Ag   2
   Department of Aeronautics and Astronautics
   Naval Postgraduate School
   Monterey, CA 93943

6. Professor Hyochoong Bang, Code AA/Ba   1
   Department of Aeronautics and Astronautics
   Naval Postgraduate School
   Monterey, CA 93943

7. LCDR Mark Feuerstein USN   1
   P.O. Box 1127
   Manassas, VA 22110